Journal of Biotechnology 358 (2022) 92–101

Contents lists available at ScienceDirect

Journal of Biotechnology

journal homepage: www.elsevier.com/locate/jbiotec

Sensitive real-time on-line estimator for oxygen transfer rates in fermenters

Marshall Trout [a], Sarah W. Harcum [b,*,1], Richard E. Groff [a]

[a] Department of Electrical and Computer Engineering, Clemson University, Clemson, SC 29634, United States
[b] Department of Bioengineering, Clemson University, Clemson, SC 29634, United States

ARTICLE INFO

Keywords:
Bioprocess monitoring
K_La
Oxygen transfer rate
Oxygen uptake rate
Feeding
Bioreactor

ABSTRACT

Recombinant *Escherichia coli* grown in large-scale fermenters are used extensively to produce plasmids and biopharmaceuticals. One method commonly used to control culture growth is predefined glucose feeding, often an exponential feeding profile. Predefined feeding profiles cannot adjust automatically to metabolic state changes, such as the metabolic burden associated with recombinant protein expression or high-cell density associated stresses. As the culture oxygen consumption rates indicates a culture's metabolic state, there exist several methods to estimate the oxygen uptake rate (OUR). These common OUR methods have limited application since these approaches either disrupt the oxygen supply, rely on empirical relationships, or are unable to account for latency and filtering effects. In this study, an oxygen transfer rate (OTR) estimator was developed to aid OUR prediction. This non-disruptive OTR estimator uses the dissolved oxygen and the off-gas oxygen concentration, in parallel. This new OTR estimator captures small variations in OTR due to physical and chemical manipulations of the fermenter, such as in stir speed variation, glucose feeding rate change, and recombinant protein expression. Due its sensitivity, this non-disruptive real-time OTR estimator could be integrated with feed control algorithms to maintain the metabolic state of a culture to a desired setpoint.

1. Introduction

Escherichia coli are used extensively in industry to produce both biopharmaceuticals and plasmids (Baeshen et al., 2015; Walsh, 2018). *E. coli* can grow rapidly on inexpensive media and are easily modified genetically (Swartz, 2001). In current practice, most industrial and benchtop fermenters use simple control strategies, specifically, closed loop proportional-integral-differential (PID) control for environmental variables such as pH, temperature, and dissolved oxygen (DO). Glucose feeding for fed-batch cultures commonly uses a preset exponential feeding schedule (Korz et al., 1995). Yet, these feeding practices are often developed to operate without any input from common on-line sensor measurements, such as the DO and off-gas oxygen concentrations (Chen et al., 1995). Both DO and off-gas oxygen concentrations are indicative of culture metabolic state. Specifically for *E. coli*, efficient growth and recombinant protein production occurs when glycolysis and the tricarboxylic acid (TCA) cycle are balanced (Gonzalez et al., 2017; Korz et al., 1995; Wolfe, 2005; Xu et al., 1999). When the glycolysis flux is higher than the TCA cycle maximum flux, acetate accumulates, even in the presence of sufficient oxygen (Sharma et al., 2007). This metabolic state is commonly called overflow metabolism (Johnston et al., 2003; Xu et al., 1999). Further, acetate accumulation is known to inhibit growth and recombinant protein production yield (Sharma et al., 2007; Xu et al., 1999). Thus, overflow metabolism is best avoided for high cell density cultures (Korz et al., 1995). To avoid overflow metabolism, the glycolytic flux, via controlled glucose feeding, need to balance the TCA cycle flux.

Currently, there are no direct method to measure the metabolic state of a culture, so surrogates are used, such as the growth rate, glucose consumption rate, and oxygen uptake rate (OUR). Standard practices require off-line assessment of cell densities over time to evaluate growth rates. There are new tools to measure glucose on-line; however, most fermentations still rely on off-line glucose measurements to assess the glucose consumption rate. There are several approaches to obtain OUR, which can be divided into three approaches: 1) dynamic, 2) global mass balance, and 3) stationary liquid mass balance (Martinez-Monge et al., 2019; Pappenreiter et al., 2019). These three main methods all have drawbacks due to underlying assumptions or operational difficulties (Bandyopa and Humphrey, 1967; Doi et al., 2020; Fontova et al., 2018; Goldrick et al., 2018; Martinez-Monge et al., 2019; Seidel et al., 2021; Van't Riet, 1979). For example, the dynamic method is disruptive as it

* Corresponding author.
E-mail address: harcum@clemson.edu (S.W. Harcum).
[1] ORCID ID: 0000-0001-9417-0489

https://doi.org/10.1016/j.jbiotec.2022.09.005
Received 3 June 2022; Accepted 12 September 2022
Available online 15 September 2022

Nomenclature

α_0	fitting parameter.
$\overline{\alpha}_0$	k_La fitting parameter, normalized to C^*_{cal}.
α_1	fitting parameter.
$\overline{\alpha}_1$	fitting parameter, normalized to C^*_{cal}.
y_0	inlet oxygen concentration (% oxygen).
$y_{0,i}$	inlet oxygen concentration at calibration (% oxygen).
y_1	bubble exiting liquid oxygen concentration (% oxygen).
y_2	headspace oxygen concentration (% oxygen).
y_3	off-gas sensor oxygen concentration (% oxygen).
C_L	liquid oxygen concentration (mg/L).
C*	liquid oxygen saturation constant (mg/L).
C^*_{cal}	liquid oxygen saturation constant at calibration (mg/L).
DO	dissolved oxygen (% saturation).
$H_g(s)$	Laplace transform of transfer function for y_0 to y_3.
$h_g(t)$	transfer function for y_0 to y_3.
k_La	volumetric oxygen mass transfer coefficient (h^{-1}).
$\overline{k_La}$	volumetric oxygen mass transfer coefficient (h^{-1}), normalized to C*cal.
M_f	mass flow rate (L/min).
N	stir speed (rpm).
OD	optical density, used as measure of cell density.
OTR	oxygen transfer rate (g/L·h).
OTR_{avg}	OTR determined from measured y_O and y_3, time-averaged by default.
OTR_{RLS}	OTR calculated by the RLS-OTR algorithm.
OUR	oxygen uptake rate (g/L·h).
P	Pressure (bar).
q_{O2}	cell specific oxygen consumption rate (g O_2/g cell·h).
R	universal gas constant (0.08314 L·bar/mol·K).
RLS	recursive least squares.
T	temperature (°C or K).
V_1	liquid volume.
V_2	headspace volume.
X	cell density (OD at 600 nm).

requires the oxygen gas flow to be stopped. Most industrial facilities will not use this method during production due to the high risk of culture loss, and will instead rely on volumetric oxygen mass transfer coefficient (k_La) values determined in buffer and extrapolated to production conditions (Doi et al., 2020). The global mass balance method uses the difference between the inlet and outlet gas concentrations, thus requires two on-line gas sensors (Fontova et al., 2018; Patel and Thibault, 2009). The stationary liquid mass balance method assumes steady-state and uses the difference between the liquid oxygen saturation constant (C*) and the measured DO (Martinez-Monge et al.; Pappenreiter et al., 2019). All three of these standard methods lack the capability to account for latency and filtering effects.

The underlying principle to reliably and precisely estimate OUR is an accurate assessment of k_La; however, real-time k_La measurements have been unreliable (Ducommun et al., 2000; Eyer et al., 1995; Nienow, 2015). One early approach to estimate k_La was the empirical Van't Riet (1979) equation. This approach estimates k_La from the power per volume ratio, superficial gas velocity and three empirical constants obtained for a particular vessel (Van't Riet, 1979). Goldrick et al. (2018) used k_La to control the glucose feeding augmented with the van't Riet (1979)) equation and off-line glucose measurements (Goldrick et al., 2018; Van't Riet, 1979); however, they were forced to smooth the oxygen transfer rate (OTR) values to predict OUR. Subsequently, any time-dependent details regarding real-time OUR information were lost. Fontova et al. (2018) calculated OUR in real-time using a modified global mass balance method (alternated the gas sensor between the inlet and outlet streams); yet, assumed a constant k_La value (Fontova et al., 2018). They noted this constant k_La assumption caused error in the OUR estimates at later culture times. And, Doi et al. (2020) measured k_La_{O2} and k_La_{CO2} using the gas-out method in buffer for several bioreactor configurations (Doi et al., 2020). However, their approach neglected the interaction of cell secretions on k_La over the culture duration.

In order to obtain accurate real-time k_La estimates, the signal filtering and delays need to be described mathematically. First, the off-gas measurement is heavily filtered by gas mixing in the headspace of the bioreactor. Second, the off-gas signal is delayed due to time required for the oxygen to travel from the liquid surface to the off-gas sensor. OTR is directly related to the volumetric coefficient, k_La, such that if k_La is known, OTR can be estimated directly. Unfortunately, k_La is a complex parameter that depends on stir speed, impeller shape and dimension, bioreactor shape and dimensions, chemical characteristics of the media, viscosity, temperature, among many other parameters (Aroniada et al., 2020; Campbell et al., 2020). There is also evidence that k_La changes over the course of a fermentation (Patel and Thibault, 2009). A mathematical method to estimate k_La in real-time would allow for OTR estimates, OUR calculations, and subsequent metabolic state assessment.

In this study, a non-disruptive k_La estimator will be described that uses only commonly available sensors (off-gas and DO). This sensitive k_La estimator can continuously estimate k_La in real-time. These real-time k_La estimate can then be used to determine OTR in real-time, which subsequential can be used to calculate OUR over the culture time. A recursive least squares (RLS) approach was used, in conjugation, with a first-order gas mixing model to fit a simple model to the observed data, which is summarized as the RLS-OTR algorithm. Two recombinant *E. coli* fermentations were conducted to validate the sensitivity of the OTR estimator to fed-batch fermentation conditions. First, a fermentation with a predefined constant exponential feeding profile was used to assess the responsiveness of the OTR estimator to small glucose pulses. The second fermentation was used to assess the effect of large glucose perturbations on the OTR estimator, by causing the cells to enter the overflow metabolic state. Further, the OTR estimator was challenged by step changes in the inlet oxygen concentration. These recombinant cultures were induced and the capability to estimate OTR in stressed cultures was evaluated.

2. Materials and methods

2.1. Bacterial strain and plasmids

E. coli MG1655 were obtained from the American Type Culture Collection (ATCC, Manassas, VA, USA). The plasmid pTVP1GFP (gift from A. Villaverde) encodes the VP1 capsid of foot-and mouth disease (Liu et al., 2006) fused to green fluorescent protein (GFP) (Garcia--Fruitos et al., 2007). *E. coli* MG1655 were transformed with the pTVP1GFP plasmid (Baig et al., 2014).

2.2. Culture conditions

E. coli MG1655 pTVP1GFP were cultured in a minimal medium described previously (Korz et al., 1995; Sharma et al., 2007). Frozen stock (1 mL, stored at −80 °C) were thawed and added to the minimal medium containing 40 mg/L ampicillin (ThermoFisher). Cells were grown overnight in a shaker incubator (C24, New Brunswick Scientific, Inc.) at 37 °C and 250 rpm. Cell densities (OD) were obtained at 600 nm with a spectrophotometer (Spectronic 30 Genesys), where 1 OD is equivalent to 0.45 g dry cell weight per liter. Samples were diluted with

deionized water to obtain absorbance readings in the linear range (0–0.45 OD). The shake flasks at approximately 2.5 OD, and still in the exponential phase, were used to inoculate the fermenters.

2.3. Fermenter operation

Fermentations were conducted in a 5-L BioStatB fermenter (Sartorius, Bethlehem, PA). Defined batch medium and feed medium were described previously in Korz et al. (1995) with the modifications described by Sharma et al. (2007). The temperature and pH were controlled by the BiostatB DCU controller. The pH and temperature during the fermentations were maintained at 6.90 and 37 °C, respectively. A solution of 20 % ammonium hydroxide was used for pH control. All cultures were induced with 1.0 mM IPTG (isopropyl-β-thiogalactopyranoside) in the fed-batch phase at approximately 35 OD. Silicone tubing (LS14, Cole-Parmer) was used for all connections with the bioreactor, which resulted in a maximum flowrate of 20 mL/min. The pre-defined exponential feed rate was 0.28 h^{-1} for both fermentations; however, the second fermentation had several planned glucose feeding perturbations.

2.4. Data collection

Matlab (Mathworks, US) was used to collect data and designate setpoints for stir speed and the feed rates, as well as perform the RLS-OTR calculations. The stir speed was used to maintain a DO setpoint of 60 %, unless stated otherwise. The BiostatB pump speeds are discretized into 2 % increments, thus, a pump dithering protocol was used to smooth this quantization. The MFCS OPC software (Sartorius) was used to communicate between Matlab and the MFCS data acquisition software (Sartorius). Gas flow rates (0–5 L/min) to the bioreactor was controlled using GFC 17 mass flow controllers (Aalborg, Germany). The off-gas measurements, such as pressure, gas temperature, and oxygen concentration, were collected by a BlueInOne Ferm 1050 (BlueSens, Germany).

3. Theory and calculations

The OTR estimator uses the input oxygen concentration (y_0), off-gas sensor oxygen concentration (y_3), oxygen concentration in the liquid (C_L) measured as DO, volumetric gas flow rates (M_f), liquid volume (V_1), and stir speed (N) measurements from the bioreactor to calculate in real-time k_La. OTR is then estimate from k_La, and subsequentially could be used to determine OUR. The RLS-OTR algorithm calculations are summarized following the theoretical equations.

3.1. OTR via off-gas measurements

Fig. 1**A** shows the physical locations within the fermenter for the parameters used to estimate k_La. The oxygen mole ratio y_i of gas are shown as it passes through the bioreactor (shown as the molar oxygen percentage (%) in subsequent figures): y_0 for the input gas, y_1 for bubbles as these leave the media, y_2 for the fully mixed headspace gas, and y_3 for the off-gas sensor measurement. Note that in this present work, y_0 is calculated from the mass flow of the input gas sources. This approach could be modified to use a inlet gas sensor measurement, if available. *OTR* can, in theory, be calculated directly from mole ratios y_0 and y_1 described in Eq. (1); however, a direct measurement of y_1 is generally not possible.

$$OTR = \frac{M_f P}{V_1 RT}(y_0 - y_1) \tag{1}$$

where P is the headspace pressure, T is temperature, and R is the universal gas constant. In the global mass balance method, y_1 is simply replaced in Eq. (1) with the off-gas sensor measurement y_3 (Patel and Thibault, 2009) and shown as

$$OTR_{avg} = \frac{M_f P}{V_1 RT}(y_0 - y_3) \tag{2}$$

The global mass balance method to determine OTR represents a time-averaged estimate of OTR (written here as OTR_{avg}), since it neglects the filtering effects of headspace mixing and the sensor dynamics. To account for these latency and filtering effects, in this work, the headspace and sensor dynamics are explicitly modeled. The headspace mixing is modeled as

$$\frac{dy_2}{dt} = \frac{M_f}{V_2}(y_2 - y_1) \tag{3}$$

where V_2 is the headspace volume. The off-gas sensor dynamics are modeled as a first order reaction

$$\frac{dy_3}{dt} = \frac{1}{\tau_2}(y_3 - y_2) \tag{4}$$

where τ_2 is the time constant associated with the sensor. The transport delay for gas to move from the bioreactor to the sensor was found to be negligible for the current system, yet this effect could be readily added to the model for larger systems or shared off-gas sensors. From Eq. (3) and Eq. (4), the Laplace-domain transfer function from y_1 to y_3 is given by

$$H_g(s) = \frac{1}{\left(\left(\frac{V_2}{M_f}\right)s + 1\right)(\tau_2 s + 1)} \tag{5}$$

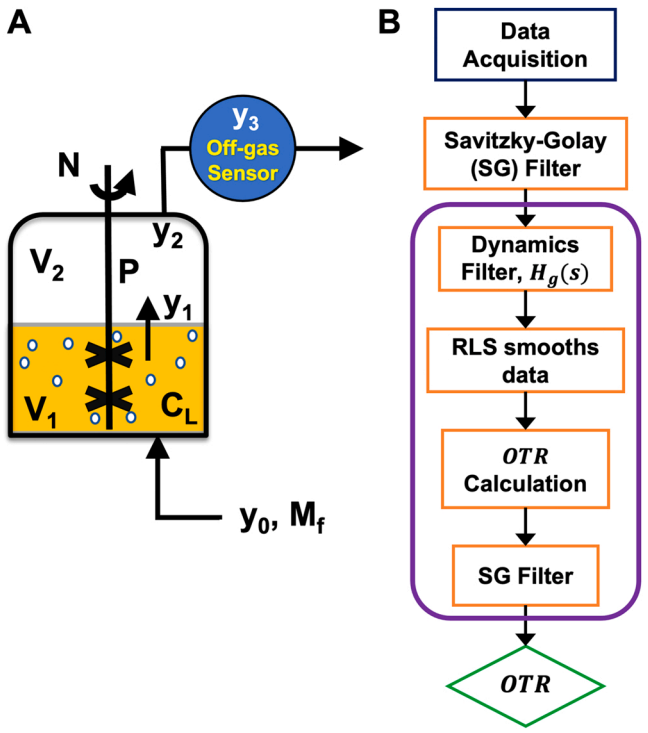

Fig. 1. Bioreactor schematic and RLS-OTR algorithm flow diagram. A) Bioreactor schematic with positions of key parameters indicated. y_0 – oxygen concentration entering the bioreactor (inlet oxygen concentration, % oxygen); y_1– oxygen concentration in the bubbles exiting the liquid (% oxygen); y_2– oxygen concentration of the gas leaving the bioreactor (% oxygen); y_3– oxygen concentration at the off-gas sensor (% oxygen); M_f – mass flowrate of y_0; V_1–liquid volume; V_2–headspace volume; and N–stir speed (rpm). B) Calculation flow diagram for the RLS-OTR algorithm. Data is acquired from the bioreactor and off-gas sensor and processed by the RLS-OTR algorithm in Matlab. A Savitsky-Golay (SG) filter is used to reduce signal noise. The reduced noise data is then convolved to determine y_1. A second SG filter is used to calculate the final OTR estimate.

where y_3 can be estimated by $H_g(s) * y_1$. Note: this notation represents the time domain input signal b_1 is filtered by the system represented by $H_g(s)$ to give time-domain output signal y_3.

3.2. OTR via oxygen concentration measurements

OTR can also be theoretically calculated from the liquid oxygen concentration (C_L), as shown in Eq. (6).

$$OTR = k_L a(C^* - C_L) \tag{6}$$

where $k_L a$ is the volumetric mass transfer coefficient, and C^* is the saturation oxygen concentration. C^* depends on the inlet gas oxygen concentration (y_0). How C_L changes with time is a function of OTR and OUR given by Eq. (7) (neglecting dilution effects).

$$\frac{dC_L}{dt} = k_L a(C^* - C_L) - OUR \tag{7}$$

Thus, if $k_L a$ is known, OTR can be calculated directly from the liquid oxygen concentration using Eq. (6). Unfortunately, $k_L a$ depends on many physical parameters that vary through time. There are several methods to estimate $k_L a$, such as the Van't Riet's (1979) equation. In this work, $k_L a$ will be modeled as linearly related to stir speed (N)

$$k_L a = \alpha_0 + \alpha_1(N - N_0) \tag{8}$$

where N_0 is an arbitrary constant used to center the model (Wang et al., 2014). The parameters α_0 and α_1 are continuously calibrated to account for the dependence of $k_L a$ on other unmeasurable physical parameters.

3.3. OTR via DO sensor measurements

At the beginning of a fermentation trial, the input gas oxygen concentration is $y_{0,cal}$, the corresponding saturated oxygen concentration of the media is C^*_{cal}, and the *DO* measurement is calibrated to 100 % at this concentration. DO measurements do not suffer from the headspace mixing and slower sensor dynamics of off-gas measurements, so estimating OTR from dissolved oxygen is more responsive than using the global mass balance off-gas calculation. Due to the calibration with air, DO measurements are related to oxygen concentration by, and not identical to the liquid concentration (C_L)

$$C_L = C^*_{cal}\frac{DO}{100} \tag{9}$$

If the input oxygen concentration is changed, then by Henry's law, the saturation concentration is

$$C^* = C^*_{cal}\frac{y_0}{y_{0,cal}} \tag{10}$$

Substituting Eq. (8), Eq. (9) and Eq. (10) into Eq. (6) allows OTR to be estimated online

$$OTR = (\overline{\alpha}_0 + \overline{\alpha}_1(N - N_0))\left(\frac{y_0}{y_{0,cal}} - \frac{DO}{100}\right) \tag{11}$$

where $\overline{\alpha}_0 = C^*_{cal}\alpha_0$ and $\overline{\alpha}_1 = C^*_{cal}\alpha_1$. If $\overline{\alpha}_0$ and $\overline{\alpha}_1$ are known, then OTR can be calculated from percentage DO measurements without the needed to know C^*_{cal}. Eq. (11) suggests the definition

$$\overline{k_L a} = \overline{\alpha}_0 + \overline{\alpha}_1(N - N_0) \tag{12}$$

which differs from $k_L a$ by a factor of C^*_{cal}.

3.4. Matching OTR off-gas and OTR dissolved oxygen

The OTR value is identical whether calculated from oxygen mole ratios Eq. (1) or from dissolved oxygen concentrations Eq. (11). Therefore, setting Eq. (1) and Eq. (11) equal allows one to solve for the unmeasurable oxygen concentration y_1 as

$$\hat{y}_1 = y_0 - \frac{V_1 RT}{M_f P}(\overline{\alpha}_0 + \overline{\alpha}_1(N - N_0))\left(\frac{y_0}{y_{0,cal}} - \frac{DO}{100}\right) \tag{13}$$

where the $\hat{y}_1$ indicates that the quantity is calculated from DO rather than measured directly. Since $H_g(s) * \hat{y}_1$ predicts the off-gas measurement y_3 based on DO measurement, $H_g(s) * \hat{y}_1$ is set equal to y_3 and rearrange where the unknown parameters $\overline{\alpha}_0$ and $\overline{\alpha}_1$ are placed on the right hand side of the equation, given as

$$\begin{aligned}(H_g(s) * y_0 - y_3) = H_g(s) * \left(\frac{V_1 RT}{M_f P}\left(\frac{y_0}{y_{0,i}} - \frac{DO}{100}\right)\right)\overline{\alpha}_0 + H_g(s) \\ * \left(\frac{V_1 RT}{M_f P}(N - N_0)\left(\frac{y_0}{y_{0,i}} - \frac{DO}{100}\right)\right)\overline{\alpha}_1\end{aligned} \tag{14}$$

Eq. (14) can be solved using least squares for the unknown parameters $\overline{\alpha}_0$ and $\overline{\alpha}_1$. Conceptually, the parameters $\overline{\alpha}_0$ and $\overline{\alpha}_1$ are fit so that OTR calculated from DO using Eq. (8) matches the ideal OTR from Eq. (1) without ever having direct access to the unmeasurable signal y_1.

3.5. Recursive least squares formalism

In the present work, the $\overline{\alpha}_0$ and $\overline{\alpha}_1$ parameters are calculated on-line using the recursive least squares (RLS) algorithm, which allows the parameters to account for the effects of other slowly evolving parameters on $k_L a$. For more detail on RLS, see Sections 3.5 and 3.6 and Simon (2006). Since Eq. (14) is only a function of two variables, $\overline{\alpha_0}$ and $\overline{\alpha_1}$, this calculation method will be referred to as the RLS-OTR algorithm, and represented as OTR_{RLS} to indicate that the RLS-OTR algorithm was used (Fig. 1**B**). M_f, P, V_1, and T are all assumed to be relatively constant for this calculation. The matrices used for the RLS algorithm method are:

$$Ax = Y \tag{15}$$

$$Y = \left[\frac{M_f P}{V_1 T}(H_g(s) * y_0 - y_3)\right] \tag{16}$$

$$A = \left[H_g(s) * \left(\frac{y_0}{y_{0,i}} - \frac{DO}{100}\right) \quad H_g(s) * (N - N_0)\left(\frac{y_0}{y_{0,i}} - \frac{DO}{100}\right)\right] \tag{17}$$

$$x = [\overline{\alpha_0} \quad \overline{\alpha_1}]^T \tag{18}$$

Where $\overline{\alpha_0}$ and $\overline{\alpha_1}$ are approximated by solving the linear set or equations given as Eq. (14) to Eq. (18). With $\overline{\alpha_0}$ and $\overline{\alpha_1}$ estimated from the data and transformed to solve for y_1. This allows one to solve for $\overline{k_L a}$ by Eq. (12) and OTR_{RLS} by Eq. (11). Fig. 1**B** shows the overall logic flow diagram for the RLS-OTR algorithm.

3.6. RLS algorithm

The time varying signals $A[t]$, $x[t]$. and $Y[t]$ are defined as the sample of A, x, and Y, respectively, at time t. To initialized the RLS algorithm, $A[0]$, $Y[0]$, and $x[0]$ were set to sized zero matrix as shown in Eqs. (19), (20) and (21):

$$A[0] = [0 \quad 0] \tag{19}$$

$$Y[0] = [0] \tag{20}$$

$$x[0] = [0 \quad 0] \tag{21}$$

To implement the RLS algorithm, a forgetting factor, λ, the Kalman gain matrix, $k[t]$, and a matrix $P[t]$ were needed. For this work, $\lambda = 0.95$ was selected; however, this parameter could be tuned to specific applications. The $k[t]$ and $P[t]$ matrices were initialized to $k[0]$ and $P[0]$ as

shown in Eqs. (22) and (23):

$$k[0] = [0 \quad 0] \tag{22}$$

$$P[0] = \begin{bmatrix} 1 & 0 \\ 0 & 1 \end{bmatrix} \tag{23}$$

The $k[t]$ and $P[t]$ equations were then calculated on-line using Eqs. (24), (25) and (26) to estimate $x[t]$, which contained the estimates of the fitting parameters, $\overline{\alpha_0}$ and $\overline{\alpha_1}$.

$$k[t] = \frac{P[t-1]A[t]}{\lambda + \quad A^T[t]P[t-1]A^T[t]} \tag{24}$$

$$P[t] = \quad \lambda^{-1}P[t-1] + \quad k[t]A^T[t]\lambda^{-1}P[t-1] \tag{25}$$

$$x[t] = x[t-1] + k[t](Y[t] - A^T[t]x[t-1]) \tag{26}$$

4. Results and discussion

Two fermentations were conducted to characterize and compare the developed OTR estimator (OTR_{RLS}) with a standard OTR (OTR_{avg}) calculation method provided by the Bluesens (Germany) off-gas sensor software. In this work, OTR_{avg} is a modified version of the global mass balance method, as the inlet oxygen concentration is calculated instead of measured (Patel and Thibault, 2009). The first fermentation used a constant exponential feed profile with an exponential rate ($\mu = 0.28\ h^{-1}$) that was maintained the entire fermentation. The second fermentation used the same predefined exponential feed profiles, but the glucose feed pump was pulsed to create substantial perturbations. The constant exponential feed fermentation was used to evaluate the OTR estimator sensitivity to small glucose pulses. The perturbed exponential feed fermentations characterized the OTR estimator responses to step changes in the inlet oxygen concentration and to overflow metabolism. Since both fermentations were induced to express the recombinant protein, the capability to estimate k_La for stressed cells was characterized (Bentley and Kompala, 1989).

The growth and glucose feed pump flow rate profiles for the two experimental fed-batch fermentations are shown in Fig. 2. Both cultures performed well and reached over 100 OD (128 and 106 OD, respectively, for the constant and perturbed exponential feed protocols). The cultures had different inoculum concentrations that resulted in shifted feed profiles for the transition from batch to fed-batch modes. The glucose feed started when the initial media glucose (5 g/L) was depleted, which aligned with the cell densities reaching approximately 5 OD. The transition from batch to fed-batch occurred at 9-h for the constant exponential feed fermentation and at 12.4-h for perturbed exponential feed fermentation. Induction was at 13 h (25.2 OD) for the constant exponential feed and 17 h (37.5 OD) for the perturbed exponential feed culture. The initial stir speed was 600 rpm for both cultures which resulted in high DO values.

The RLS-OTR algorithm was used to determine k_La, and then OTR (OTR_{RLS}). For comparison, the global mass-transfer OTR (OTR_{avg}) presented in Eq. (2) was calculated, as well. These OTR comparisons are shown for the constant exponential feed cultures in Fig. 3. Since RLS-OTR calculations are dependent on y_0, y_3, DO, and stir speed, these time profiles have also been included in Fig. 3. As the cell density increased it was necessary to enrich the inlet gas stream with oxygen in order to maintain the DO. Unfortunately, the manually selected initial enrichment levels only required the oxygen mass flow controllers to operate near its lower calibration range. The low enrichment levels caused y_0 to oscillate. Thus between 10 and 14 h (Fig. 3**C**), and as a result, the corresponding OTR estimates were not reliable during this time (Fig. 3**A**). These step changes in the y_0 profile are readily observable (Fig. 3**C**). Once the oxygen mass flow controller was set to higher gas flow rates (≥20 % enrichment), the OTR estimates stabilized. Over the course of the experiment, both algorithms were able to make OTR

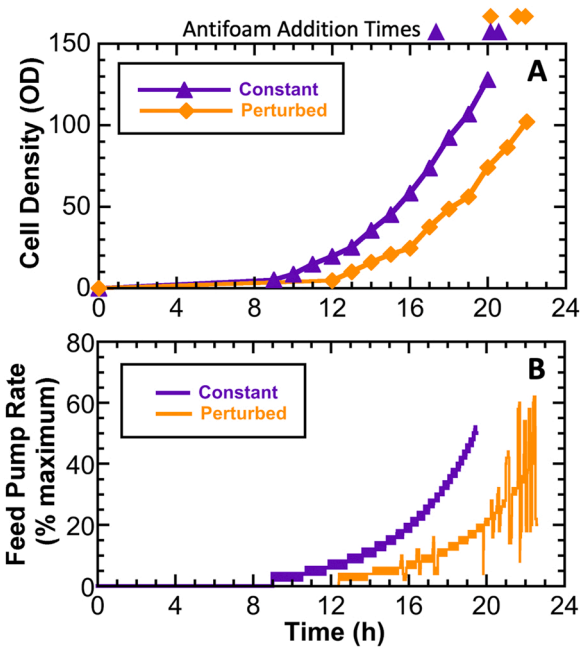

Fig. 2. Growth and glucose feed rate profiles for the constant and perturbed exponential fed-batch recombinant *E. coli* fermentations. **A)** Cell density (OD); **B)** feed pump rate (% of maximum speed, where 100 % equals 20 mL/min). The first fermentation used a constant predefined exponential feed rate to control the culture growth rate to 0.28 h^{-1}. The fed-batch phase began at 9 h with induction at 13 h. Antifoam additions are indicated by the purple triangles above panel A. The second fermentation used a predefined exponential feed rate to control the growth rate to 0.28 h^{-1}; however, large glucose flow rate changes were used to perturb the culture. The fed-batch phase began at 12.4 h with induction at 15 h. Antifoam additions are indicated by the purple triangles (constant) or orange diamonds (perturbed) above panel A.

estimates despite the high degree of variability in the DO and stir speed, and both algorithms predicted OTR to increase with increasing cell densities. When the inlet gas composition changes, the OTR_{avg} estimate spikes, as can be clearly observed at hours 16, 17, and 17.5 h. These spikes could be reduced or eliminated by replacing the y_0 with $H_g(s) * y_0$ in the global balance method Eq. (2), so that the inlet gas measurement is filtered similarly to y_3. OTR_{RLS} is minimally affected by changes in inlet gas, because this algorithm already accounts for headspace filtering and sensor dynamics. At the resolution of the entire fermentation, it is difficult to fully appreciate the latency and filtering effects captured by OTR_{RLS}, but not by OTR_{avg}.

To highlight the differences in the OTR_{RLS} and OTR_{avg} responses, the time period from 15.4 to 15.65 h (15 min) is shown in Fig. 4 for the constant exponential feed fermentation. For the time period shown, the pump speed value for the predefined exponential feed profile was 17 % (3.4 mL/min). Due to the operational limits of the BiostatB DCU pumps, only even-numbered percentages can be obtained, despite an odd-numbered setting. To approximate odd-numbered percentages, a dithering algorithm was developed that alternates between consecutive even-numbers. The OTR response to 2 % pump speed changes were captured by the OTR_{RLS} algorithm as slope changes, shown in Fig. 4**A**. As the predefined exponential profile was set to be 0.28 h^{-1}, the feed rate is considered to be below the maximum TCA cycle flux of 0.30 h^{-1} (Xu et al., 1999). At this point in the culture, the cells were in the oxidative metabolic state for pump speeds of 16 % and 18 %. Consequently, small changes in the glucose flux, controlled by the glucose feed pump flow rate, resulted in OUR changes due to the TCA cycle, and these OUR changes are detected as OTR changes. In the present work, OUR is essentially equal to OTR because the magnitude of the dC_L/dt term in Eq. (7) is very small in comparison to OUR and OTR. In the following

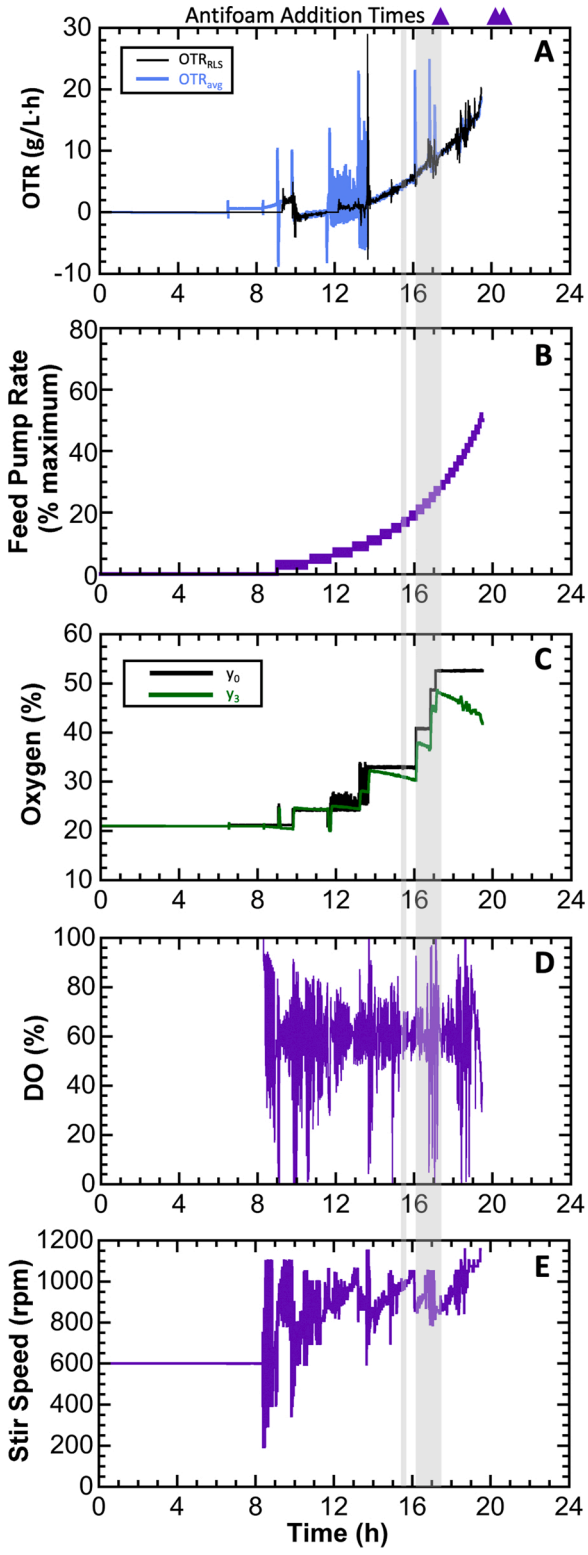

Fig. 3. OTR response for the constant exponential fed-batch culture. **A)** OTR estimated using the RLS-OTR algorithm which accounts for latency and filtering effects (OTR_{RLS}) and OTR estimated using the modified global mass balance method (OTR_{avg}). **B)** Glucose feed pump flow rate; **C)** Inlet (y_0) and off-gas sensor (y_3) oxygen concentrations; **D)** Dissolved oxygen (DO); and **E)** stir speed. The fed-batch phase began at 9 h and induction occurred at 13 h. Antifoam additions occurred at 17.15, 19.8, and 20.2 h, and these times are indicated by purple triangles above panel A. The grey boxes highlight the times to be presented in Figs. 4 and 5.

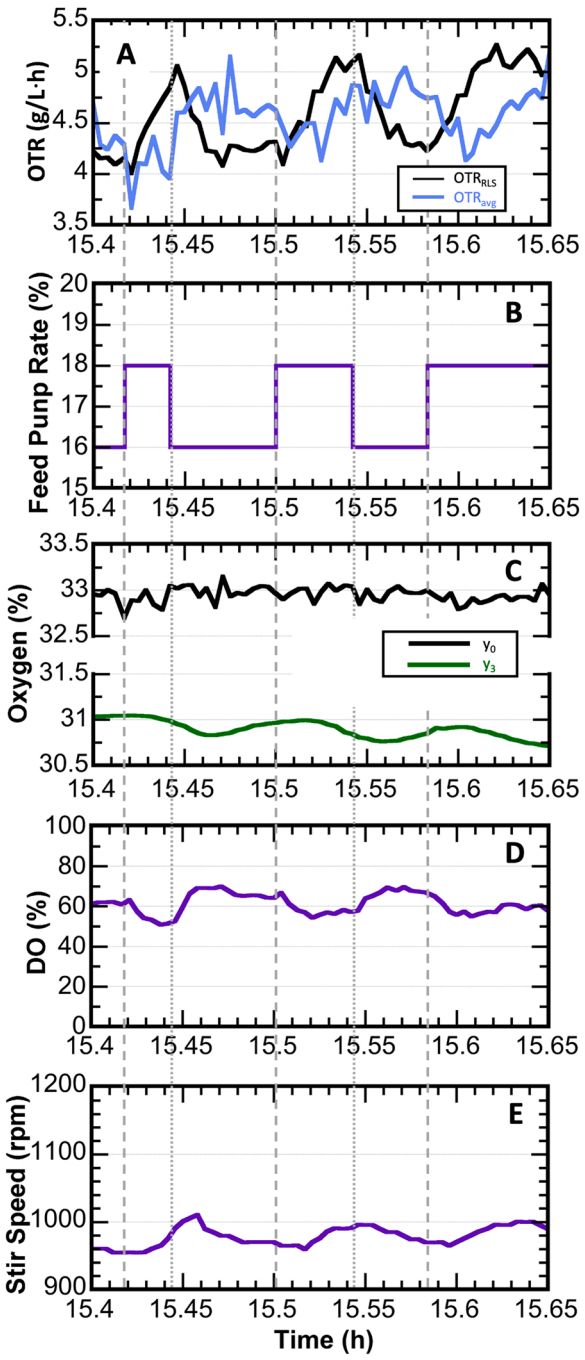

Fig. 4. OTR responses to small glucose flux variations for the constant exponential fed-batch culture. **A)** OTR estimated using the RLS-OTR algorithm which accounts for latency and filtering effects (OTR_{RLS}) and OTR estimated using the modified global mass balance method (OTR_{avg}). **B)** Glucose feed pump flow rate; **C)** Inlet (y_0) and off-gas sensor (y_3) oxygen concentrations; **D)** Dissolved oxygen (DO); and **E)** stir speed. To approximate 17 % feeding, the pump was dithered between 16 % and 18 %, as the controller was only capable of even numbered intervals. The vertical dashed lines indicate when the glucose feed pump flow rate was increased and the dotted line indicates when the glucose feed pump flow rate was decreased.

discussion, we will treat OTR and OUR as equal. That is, an increase in OUR is associated with an equal increase in OTR, and vice versa. When the glucose feed pump was increased from 16 % to 18 % at 15.42 h, the OTR_{RLS} increased immediately until the glucose pump flow rate was decreased. When the glucose pump feed flow rate was decreased from 18 % to 16 % at 15.44 h, OTR_{RLS} decreased due to OUR decreasing.

These OTR responses confirm the culture was in oxidative metabolism. The OTR_{avg} method noticeably lags the pump flow rate changes, which would confound OTR being used for feed control, as the likelihood of overfeeding is possible during the lag. The RLS-OTR algorithm demonstrated its capability to detect small OUR changes for cultures in an oxidative metabolic state.

Since high-cell density *E. coli* cultures require air enrichment with oxygen to maintain acceptable DO values, an OTR estimator must have the capability to provide accurate estimates across oxygen concentration step changes. Fig. 5 shows the OTR, glucose feed pump flow rate, and inlet and outlet oxygen concentrations from 16 to 17.5 h for the constant exponential feed fermentation. At this scale, the close alignment of the glucose pump and the inlet oxygen concentration changes can be observed. For the first inlet oxygen concentration step change at approximately 16.1 h, there was a coinciding glucose pump flow rate decrease. Yet, the OTR_{RLS} profile quickly responded and adjusted to the inlet gas concentration change and decreased due to the lower glucose flux. In contrast, the OTR_{avg} profile dramatically increased (overshooting by 5-fold) and took approximately 6 min to stabilize.

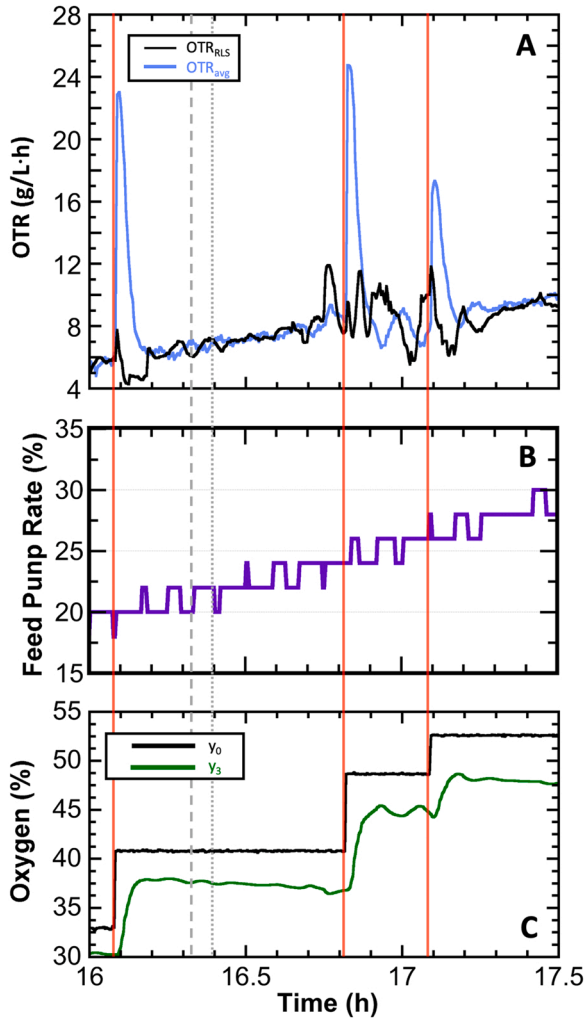

Fig. 5. OTR responses to oxygen enrichment for the constant exponential fed-batch culture. **A)** OTR estimated using the RLS-OTR algorithm which accounts for latency and filtering effects (OTR_{RLS}) and OTR estimated using the modified global mass balance method (OTR_{avg}). **B)** Glucose feed pump flow rate; **C)** Inlet (y_0) and off-gas sensor (y_3) oxygen concentrations. The vertical dashed line indicates an example where the glucose feed pump flow rate was increased and the dotted line indicates an example where the glucose feed pump flow rate was decreased. The vertical red lines indicate when the oxygen enrichment increased.

Additionally, the glucose flow rate changes between 16.3 and 16.4 h were captured by the OTR_{RLS} algorithm, whereas the OTR_{avg} method resulted in a lagged profile. Further, the 2nd and 3rd inlet gas concentration step changes also resulted in overshooting and delayed behavior for the OTR_{avg} method, while the OTR_{RLS} algorithm was responsive to the glucose flux variations. Thus, the OTR_{RLS} algorithm is capable of accurate OTR predictions across inlet oxygen concentration step changes.

Cultures in overflow metabolism would not have observable OUR changes due to sudden increases or decreases in the glucose flow since the TCA cycle is saturated (Korz et al., 1995). For glucose pump flow rate decreases to elicit an OTR response, excess glucose must first be consumed, such that the glucose flux falls below the maximum TCA cycle flux (Carneiro et al., 2013; Korz et al., 1995; Pepper et al., 2014; Wang et al., 2014). This overflow phenomena would be observed as a lag in the OTR response following a glucose flux decrease. Only once the cells consume all the excess glucose, the OUR will decrease, observed as a OTR decrease under control DO. The perturbed exponential feed fermentation was conducted to characterize the RLS-OTR algorithm response to a shift from overflow to oxidative metabolic states. OTR profiles calculated by the RLS-OTR algorithm and global mass transfer equation (OTR_{avg}) are shown in Fig. 6 for the entire fermentation. The glucose feed pump flow rates are shown, as the glucose flux directly impacts the metabolic state of the culture. Also, y_0, y_3, DO, and stir speeds are shown in Fig. 6, as these are used in the RLS-OTR algorithm, and y_0 and y_3 are used by the OTR_{avg} method. The minimum oxygen enrichment was set to 20 % to eliminate the oscillation in b_0 encountered during the constant exponential feed fermentation. At first glance, the OTR_{avg} values appear more stable than those from the RLS-OTR algorithm; however, the closer examination shows that the OTR_{avg} estimate is filtering out important culture dynamics.

To evaluate the RLS-OTR algorithm under a metabolic shift, the glucose feed pump flow rates were varied for the constant exponential feed profile setpoints. The small glucose flux variations used were between 15 and 20 h failed to put the culture into overflow metabolism. The larger glucose flux variation after 20 h were able to cause overflow metabolism. In order to visual these OTR responses, Fig. 7 highlights the time period from 22 to 22.6 h. The culture remained in oxidative metabolism during an initial glucose flux step increase at 22.08 h. The subsequent glucose flux step increase at 22.17 h pushed the culture into overflow metabolism, as observed in the OTR_{RLS} response by the flat (saturated) profile. When the glucose feed pump flow rate was decreased at 22.26 h, the OTR_{RLS} profile remained elevated, indicating that the TCA cycle remained saturated. Then at 22.3 h, the OTR_{RLS} profile decreased, indicating the excess glucose had been consumed and OUR was decreasing. The next glucose pulse at 22.34 h caused OTR_{RLS} profile to increase, and overflow metabolism was reached by 22.42 h, as indicated by the flat OTR_{RLS} profile. When the glucose feed pump flow rate was decreased at 22.5 h, the culture was again in overflow metabolism until 22.58 h, at which time the excess glucose was consumed and OTR_{RLS} decreased. For OTR_{avg} method, it was not possible to clearly define these metabolic phase shifts, as the OTR_{avg} responses lagged the glucose flux changes by $\geq$ 3 mins.

It is well-accepted that expression of a recombinant protein causes a metabolic burden. In the dynamic method for k_La estimation, it is assumed q_{O2} is a constant (Bandyopa and Humphrey, 1967; Martinez-Monge et al., 2019; Pappenreiter et al., 2019). The metabolic assessment capability gained by the RLS-OTR algorithm to measure OTR in real-time can allow for q_{O2} to be assessed as well. The q_{O2} profiles obtained for the constant and perturbed exponential feed cultures were obtained by dividing OTR_{RLS} by the predicted biomass. The predicted biomass was modeled as an exponential function to fit the off-line cell density measurements. Fig. 8 shows the q_{O2} value profiles for these two fermentations, post-induction. For both fermentations, the q_{O2} values ranged between 0.06 and 0.3 g O_2/g cell·h and increased post-induction with very similar profiles. Literature ranges for *E. coli* are between 0.32

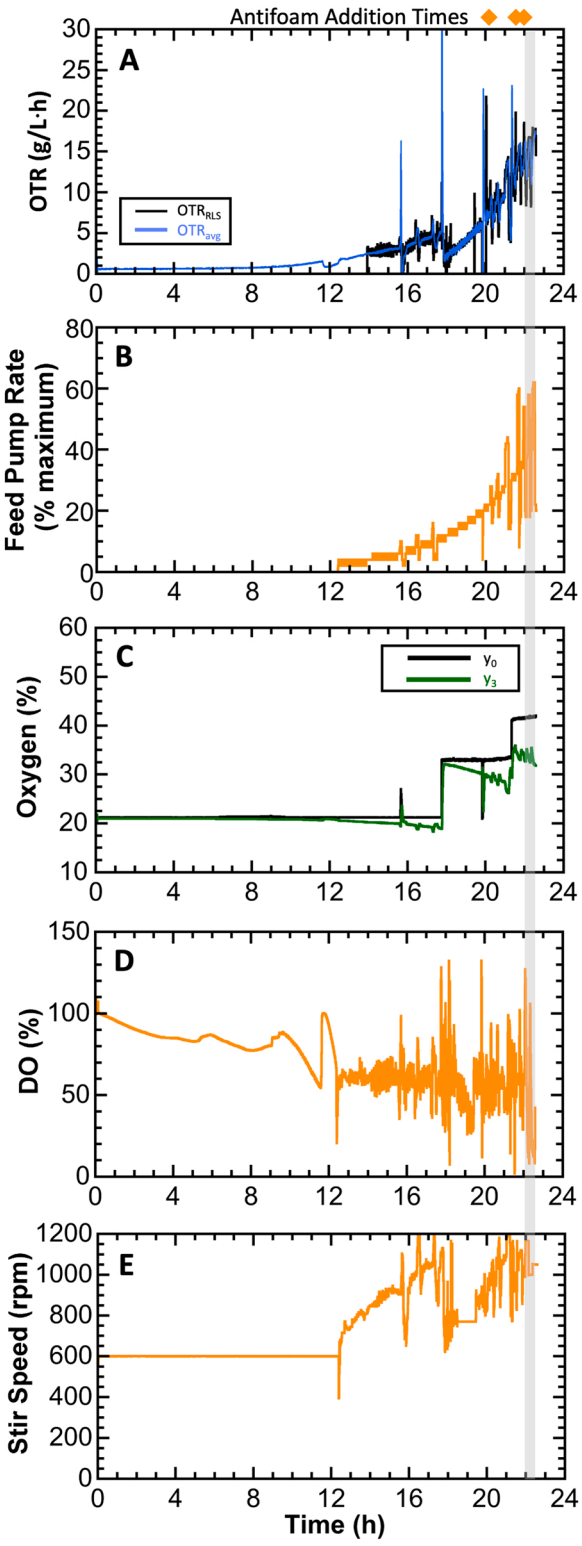

Fig. 6. OTR responses for the perturbed exponential feed culture. **A)** OTR estimated using the RLS-OTR algorithm which accounts for latency and filtering effects (OTR_{RLS}) and OTR estimated using the modified global mass balance method (OTR_{avg}); **B)** Glucose feed pump flow rate; **C)** Inlet (y_0) and off-gas sensor (y_3) oxygen concentrations; **D)** Dissolved oxygen (DO); and **E)** stir speed. To approximate 17 % feeding, the pump was dithered between 16 % and 18 %, as the controller was only capable of even-numbered intervals. The fed-batch phase began at 12.4 h and induction occurred at 17 h. Antifoam additions occurred at 19.8, 21.2, and 21.8 h, and these times are indicated by diamonds above panel A. The grey box highlights the time to be presented in Fig. 7.

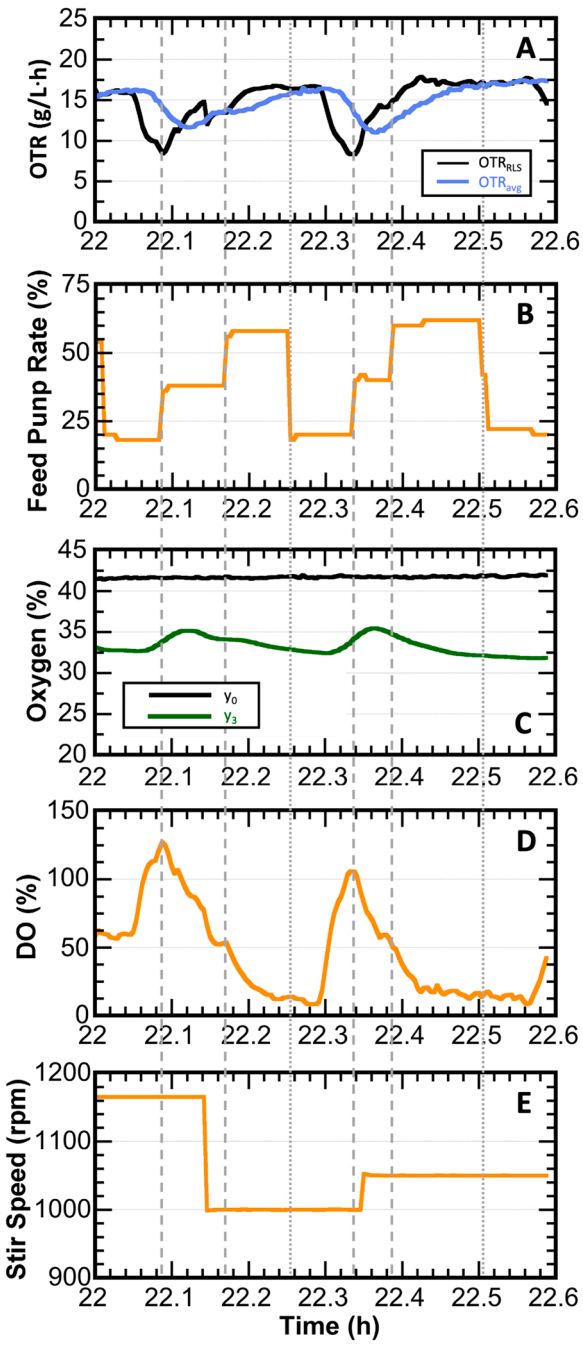

Fig. 7. OTR responses to shifts between oxidative and overflow metabolic states for the perturbed exponential fed-batch culture. **A)** OTR estimated using the RLS-OTR algorithm which accounts for latency and filtering effects (OTR_{RLS}) and OTR estimated using the modified global mass balance method (OTR_{avg}). **B)** Glucose feed pump flow rate; **C)** inlet (y_0) and off-gas sensor (y_3) oxygen concentrations; **D)** Dissolved oxygen (DO); and **E)** stir speed. The feed rate was purposely pulsed up and down to characterize the OTR response to overflow and oxidative metabolism. The vertical dashed lines indicate when the glucose feed pump flow rate was increased and the dotted line indicates when the glucose feed pump flow rate was decreased.

and 0.38 g O_2/g cell·h (Shuler et al., 2017); however, it is not clear if these literature cultures were under glucose feed control or what media was used. Glucose limited cultures would have lower q_{O2} values compared to cultures grown with excess glucose; cultures in rich media would have higher q_{O2} values. For fed-batch *E. coli*, q_{O2} has been observed to range from 0.019 to 0.16 g O_2/g cell·h for recombinant, but

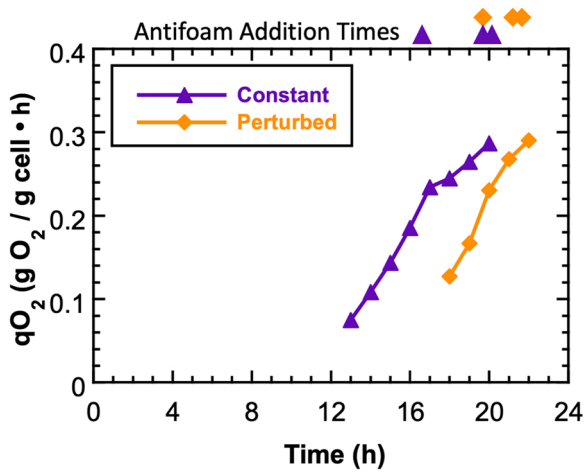

Fig. 8. Cell specific oxygen uptake rates (q_{O2}) the constant and perturbed exponential fed-batch recombinant *E. coli* fermentations. The q_{O2} values were determined from the OTR and biomass concentrations for the fermentations post-induction. Antifoam additions are indicated by the purple triangles (constant) or orange diamonds (perturbed) above panel A.

uninduced *E. coli* (Lin et al., 2001). Several models have been developed for oxygen consumption by *E. coli* (Anane et al., 2017; Seidel et al., 2021; Zeng and Yang, 2019), yet none these studies accounted the effects of the metabolic burden associated with recombinant protein expression on q_{O2}. The increasing post-induction q_{O2} values observed in this work indicate that the metabolic burden was increasing, as cells required higher amounts of oxygen under a steady growth rate. The RLS-OTR algorithm will allow for q_{O2} to be evaluated in real-time, where dynamics due to feed rates and associated metabolic burden can be characterized.

The relationship between k_La and stir speed is shown in Fig. 9 for both cultures. Each data point represents the calculation of k_La generated using the $\overline{\alpha_0}$ and $\overline{\alpha_1}$ estimates. The relationship between the estimated k_La and stir speed changes over the course of the fermentation, so k_La is different for the same stir speed at different times in the fermentation. Also, the slope of the k_La versus stir speed shifts throughout the fermentations. This shift in k_La is due to many culture events, such as cell secretion build-up, base addition accumulation, dissolved gases, antifoam additions, and submersion of additional impellers, all of which are difficult to quantify in real-time. It is clearly visible for the constant feed fed-batch cultures that the k_La-stir speed relationship was different before and after induction, as shown by the red to orange colored data points (Fig. 9**A**). Additionally, despite these cultures being well matched with respect to growth rates and cell density, the on-line estimator indicates that the k_La was significantly different even 1–2 h post-induction, as shown by the unequal k_La values in green hues. At later times post-induction, the k_La values are more similar (purple hues), most likely due to the combination of base and antifoam additions. Interestingly, the perturbed fed-batch culture k_La and stir speed have several excursions off a linear relationship (Fig. 9**B**). These excursions correspond in time to the occurrence of high or low glucose flow rates. If the van't Riet equation were used only, for example, these curves would be a single line (Van't Riet, 1979). The RLS-OTR algorithm on-line estimator allows for calculation of k_La without separately quantifying all the inputs that effect the k_La. Further, the RLS-OTR algorithm for k_La estimates is sensitive to culture changes, which will make it a value tool for closed-loop feed control.

5. Conclusions

An RLS-OTR algorithm was developed and used to estimate k_La and *OTR* on-line and in real-time using standard industrial sensors, i.e., DO

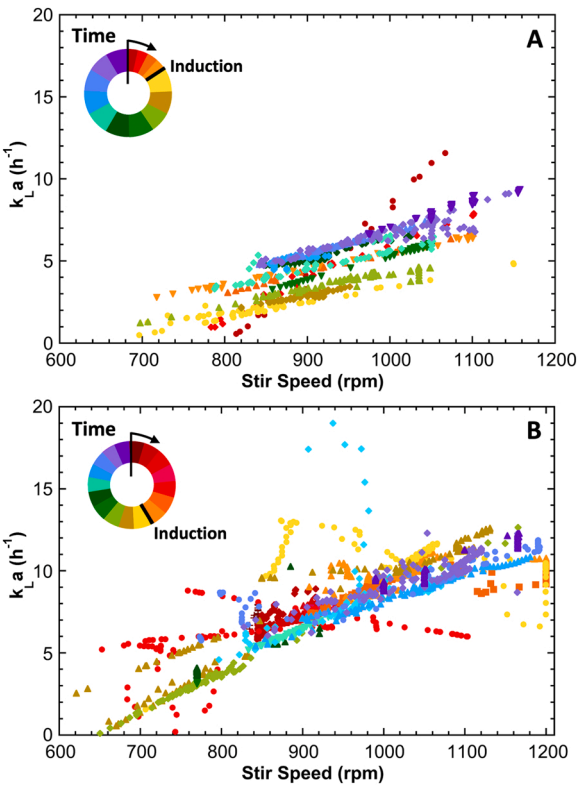

Fig. 9. Relationship between k_La and stir speed for fed-batch cultures. The rings in the upper right depict fermentation time by color, clockwise. The black line on the ring indicated the time of induction. The colors post-induction are align for the two different feeding strategies. **A)** Constant exponential fed-batch culture. For the constant exponential cultures, the smaller wedges represent 15 min intervals and the larger wedges represent 30 min intervals. **B)** Perturbed exponential fed-batch culture. For the perturbed culture, all wedges represent 30 min intervals.

and off-gas. A first-order model of gas mixing was coupled to the sensor dynamics, the inlet gas concentration and DO measurements. This resulted in a linear set of equations that could be estimated using a least-squares technique. The RLS-OTR algorithm was able to account for latency and filtering effects that occur between the inlet oxygen and the off-gas oxygen measurements. This resulted in an accurate, generalizable method to estimate *OTR* on-line and in real-time.

The RLS-OTR algorithm was compared to the OTR_{avg}, the global mass balance method for estimating OTR. The algorithms were challenged by small and large glucose feed rate variations. Additionally, the effects of step changes to the inlet oxygen sparge were evaluated. It was observed that the RLS-OTR algorithm was responsive to small glucose flux variations when the culture was in an oxidative metabolic state. In contrast, OTR_{avg} had noticeable lags. The global mass balance equation uses only the inlet and off-gas oxygen concentrations to estimate OTR, a slight modification of the global mass balance method (Martinez-Monge et al., 2019), and thus lacks the capability to account for latency and filtering effects. The effects of filtering and latency become more pronounced and problematic in systems with larger headspaces and greater distances between the fermenter and the off-gas sensor. Conversely, the RLS-OTR method was able to account for headspace volume or distance between fermenter to off-gas sensor. Thus, the RLS-OTR algorithm could be implemented in large production vessels with a shared off-gas sensor.

The k_La and stir speed relationship was determined to be variable, which was expected; nonetheless, the real-time k_La estimator was able to adjust throughout the fermentation, unlike the van't Riet correlation. As it is well-documented that k_La depends on many factors that change during a fermentation beyond geometry, such as viscosity, impeller

geometry, amount of soluble material in the media, antifoam additions etc. (Aroniada et al., 2020; Campbell et al., 2020), a dynamically updated k_La estimator is desired. While it is difficult to directly relate the changes seen in these experiments to any one factor, this study clearly shows the shift in the k_La-stir speed relationship over the course of the fermentations (Fig. 9). The feed pulse fermentations demonstrated that the RLS-OTR algorithm is capability of producing a real-time signal that contains information about the metabolic state of the culture. Information regarding the metabolic state of the culture would allow for improved feed control and lower waste product build up. Accordingly, the RLS-OTR algorithm in the future would be integrated into a feed control algorithm.

Funding

This work was supported in part by the National Science Foundation [IIP-1624641 and CBET-1218345]; and the Advanced Mammalian Biomanufacturing Innovation Center (AMBIC) industrial membership fees.

CRediT authorship contribution statement

Marshall Trout: Conceptualization, Methodology, Investigation, Software, Writing – original draft. **Sarah Harcum:** Formal analysis, Visualization, Resources, Supervision, Writing – review & editing. **Richard Groff:** Conceptualization, Software, Resources, Supervision, Writing – review & editing.

Conflicts of interest

The authors declare that they have no conflict of interest.

Data Availability

Data and Matlab programs can be made available upon request to the corresponding author.

Acknowledgments

Thomas Caldwell and Daniel Odenwelder for culture techniques, Swadeel Gaad, Shahin Lashkari, Mohammad Mayyan, Matthew Pepper, Li Wang for past work on the k_La/OTR estimator. The pTVP1GFP plasmid was generously provided by E. Garcia-Fruitos and A. Villaverde, Universitat Autònoma de Barcelona. The graphical abstract was created using Biorender.com.

References

Anane, E., Lopez, D.C.C., Neubauer, P., Bournazou, M.N.C., 2017. Modelling overflow metabolism in *Escherichia coli* by acetate cycling. Biochem. Eng. J. 125, 23–30.
Aroniada, M., Maina, S., Koutinas, A., Kookos, I.K., 2020. Estimation of volumetric mass transfer coefficient (k_La) - review of classical approaches and contribution of a novel methodology. Biochem. Eng. J. 155.
Baeshen, M.N., Al-Hejin, A.M., Bora, R.S., Ahmed, M.M.M., Ramadan, H.A.I., Saini, K.S., Baeshen, N.A., Redwan, E.M., 2015. Production of biopharmaceuticals in *E. coli:* current scenario and future perspectives. J. Microbiol. Biotechnol. 25, 953–962.
Baig, F., Fernando, L.P., Salazar, M.A., Powell, R.R., Bruce, T.F., Harcum, S.W., 2014. Dynamic transcriptional response of *Escherichia coli* to inclusion body formation. Biotechnol. Bioeng. 111, 980–999.
Bandyopa, B., Humphrey, A.E., 1967. Dynamic measurement of volumetric oxygen transfer coefficient in fermentation systems. Biotechnol. Bioeng. 9, 533.
Bentley, W.E., Kompala, D.S., 1989. A novel structured kinetic modeling approach for the analysis of plasmid instability in recombinant bacterial cultures. Biotechnol. Bioeng. 33, 49–61.
Campbell, K., Wang, J., Daigger, G.T., 2020. Filamentous organisms degrade oxygen transfer efficiency by increasing mixed liquor apparent viscosity: mechanistic understanding and experimental verification. Water Res. 173.
Carneiro, S., Ferreira, E.C., Rocha, I., 2013. Metabolic responses to recombinant bioprocesses in *Escherichia coli*. J. Biotechnol. 164, 396–408.
Chen, Q., Bentley, W.E., Weigand, W.A., 1995. Optimization for a Recombinant *E. coli* Fed-Batch Fermentation. Appl. Biochem. Biotechnol. 51/52, 449–461.
Doi, T., Kajihara, H., Chuman, Y., Kuwae, S., Kaminagayoshi, T., Omasa, T., 2020. Development of a scale-up strategy for Chinese hamster ovary cell culture processes using the k(L)a ratio as a direct indicator of gas stripping conditions. Biotechnol. Prog.
Ducommun, P., Ruffieux, P.A., Furter, M.P., Marison, I., von Stockar, U., 2000. A new method for on-line measurement of the volumetric oxygen uptake rate in membrane aerated animal cell cultures. J. Biotechnol. 78, 139–147.
Eyer, K., Oeggerli, A., Heinzle, E., 1995. Online gas-analysis in animal-cell cultivation 2. Methods for oxygen-uptake rate estimation and its application to controlled feeding of glutamine. Biotechnol. Bioeng. 45, 54–62.
Fontova, A., Lecina, M., Lopez-Repullo, J., Martinez-Monge, I., Comas, P., Bragos, R., Cairo, J.J., 2018. A simplified implementation of the stationary liquid mass balance method for on-line OUR monitoring in animal cell cultures. J. Chem. Technol. Biotechnol. 93, 1757–1766.
Garcia-Fruitos, E., Martinez-Alonso, M., Gonzalez-Montalban, N., Valli, M., Mattanovich, D., Villaverde, A., 2007. Divergent genetic control of protein solubility and conformational quality in *Escherichia coli*. J. Mol. Biol. 374, 195–205.
Goldrick, S., Lee, K., Spencer, C., Holmes, W., Kuiper, M., Turner, R., Farid, S.S., 2018. On-line control of glucose concentration in high-yielding mammalian cell cultures enabled through oxygen transfer rate measurements. Biotechnol. J. 13.
Gonzalez, J.E., Long, C.P., Antoniewicz, M.R., 2017. Comprehensive analysis of glucose and xylose metabolism in *Escherichia coli* under aerobic and anaerobic conditions by C-13 metabolic flux analysis. Metab. Eng. 39, 9–18.
Johnston, W.A., Stewart, M., Lee, P., Cooney, M.J., 2003. Tracking the acetate threshold using DO-transient control during medium and high cell density cultivation of recombinant *Escherichia coli* in complex media. Biotechnol. Bioeng. 84, 314–323.
Korz, D.J., Rinas, U., Hellmuth, K., Sanders, E.A., Deckwer, W.D., 1995. Simple fed-batch technique for high cell-density cultivation of *Escherichia coli*. J. Biotechnol. 39, 59–65.
Lin, H.Y., Mathiszik, B., Xu, B., Enfors, S.O., Neubauer, P., 2001. Determination of the maximum specific uptake capacities for glucose and oxygen in glucose-limited fed-batch cultivations of *Escherichia coli*. Biotechnol. Bioeng. 73, 347–357.
Liu, Y., Hu, R., Zhang, S., Zhang, L., Wei, X., Chen, L., 2006. Expression of the foot-and-mouth disease virus VP1 protein using a replication-competent recombinant canine adenovirus type 2 elicits a humoral antibody response in a porcine model. Viral Immunol. 19, 202–209.
Martinez-Monge, I., Roman, R., Comas, P., Fontova, A., Lecina, M., Casablancas, A., Cairo, J.J., 2019. New developments in online OUR monitoring and its application to animal cell cultures. Appl. Microbiol. Biotechnol. 103, 6903–6917.
Nienow, A.W., 2015. Mass transfer and mixing across the scales in animal cell culture. Anim. Cell Cult. 137–167.
Pappenreiter, M., Sissolak, B., Sommeregger, W., Striedner, G., 2019. Oxygen uptake rate soft-sensing via dynamic kla computation: cell volume and metabolic transition prediction in mammalian bioprocesses. Front. Bioeng. Biotechnol. 7.
Patel, N., Thibault, J., 2009. Enhanced in situ dynamic method for measuring k_La in fermentation media. Biochem. Eng. J. 47, 48–54.
Pepper, M.E., Wang, L., Padmakumar, A., Burg, T.C., Harcum, S.W., Groff, R.E., Ieee, 2014. A CMI (cell metabolic indicator)-based controller for achieving high growth Rate *Escherichia coli* cultures. 2014 36th Annu. Int. Conf. IEEE Eng. Med. Biol. Soc. 2911–2915.
Seidel, S., Maschke, R.W., Werner, S., Jossen, V., Eibl, D., 2021. Oxygen mass transfer in biopharmaceutical processes: numerical and experimental approaches. Chem. Ing. Tech. 93, 42–61.
Sharma, S.S., Campbell, J.W., Frisch, D., Blattner, F.R., Harcum, S.W., 2007. Expression of two recombinant chloramphenicol acetyltransferase variants in highly reduced genome *Escherichia coli* strains. Biotechnol. Bioeng. 98, 1056–1070.
Shuler, M.L., Kargi, F., DeLisa, M.P., 2017. Bioprocess Engineering-Basic Concepts, third ed. Prentice Hall, Boston.
Simon, D., 2006. Optimal State Estimation. Wiley and Sons, NJ.
Swartz, J.R., 2001. Advances in *Escherichia coli* production of therapeutic proteins. Curr. Opin. Biotechnol. 12, 195–201.
Van't Riet, K., 1979. Review of measuring methods and results in nonviscous gas-liquid mass-transfer in stirred vessels. Ind. Eng. Chem. Process Des. Dev. 18, 357–364.
Walsh, G., 2018. Biopharmaceutical benchmarks 2018. Nat. Biotechnol. 36, 1136–1145.
Wang, L., Pepper, M.E., Padmakumar, A., Burg, T.C., Harcum, S.W., Groff, R.E., Ieee, 2014. A real-time adaptive oxygen transfer rate estimator for metabolism tracking in *Escherichia coli* cultures. 2014 36th Annu. Int. Conf. Ieee Eng. Med. Biol. Soc. 6191–6194.
Wolfe, A.J., 2005. The acetate switch. Microbiol. Mol. Biol. Rev. 69, 12–50.
Xu, B., Jahic, M., Enfors, S.O., 1999. Modeling of overflow metabolism in batch and fed-batch cultures of *Escherichia coli*. Biotechnol. Prog. 15, 81–90.
Zeng, H., Yang, A., 2019. Modelling overflow metabolism in *Escherichia coli* with flux balance analysis incorporating differential proteomic efficiencies of energy pathways. BMC Syst. Biol. 13.